Running head: Manganese cluster assembly

Corresponding Author
Robert L. Burnap
Oklahoma State University
307 Life Science East
Stillwater, OK 74078
Phone: 405-744-7445
Email: Robert.burnap@okstate.edu

Research Category
Photosynthesis, Photosystem II, Biophysics

An amino residue that guides the correct photoassembly the water-oxidation complex but not required for high affinity Mn^{2+} binding

Anton P. Avramov, Minquan Zhang, Robert L. Burnap
Department of Microbiology and Molecular Genetics, Oklahoma State University, Stillwater, OK 74078, USA

18 **Footnotes**

19 This work was supported by the National Science Foundation; grant no. MCB-1716408

20

21 **Abbreviations:** HAS: high affinity site, HA: hydroxylamine, P680; primary electron donor of the
22 reaction center; PSII, Photosystem II; WOC, H_2O-oxidizing complex; Y_z, redox-active tyrosine secondary
23 electron donor serving as reactive interface between the primary donor and the WOC.

24

Abstract

The assembly of the Mn_4O_5Ca cluster of the photosystem II (PSII) starts from the initial binding and photooxidation of the first Mn^{2+} at a high affinity site (HAS). Recent cryo-EM apo-PSII structures reveal an altered geometry of amino ligands in this region and suggest the involvement of D1-Glu189 ligand in the formation of the HAS. We now find that Gln and Lys substitution mutants photoactivate with reduced quantum efficiency compared to the wild-type. However, the affinity of Mn^{2+} at the HAS in D1-E189K was very similar to the wild-type (~2.2 μM). Thus, we conclude that D1-E189 does not form the HAS (~2.9 μM) and that the reduced quantum efficiency of photoactivation in D1-E189K cannot be ascribed to the initial photooxidation of Mn^{2+} at the HAS. Besides reduced quantum efficiency, the D1-E189K mutant exhibits a large fraction of centers that fail to recover activity during photoactivation starting early in the assembly phase, becoming recalcitrant to further assembly. Fluorescence relaxation kinetics indicate on the presence of an alternative route for the charge recombination in Mn-depleted samples in all studied mutants and exclude damage to the photochemical reaction center as the cause for the recalcitrant centers failing to assemble and show that dark incubation of cells reverses some of the inactivation. This reversibility would explain the ability of these mutants to accumulate a significant fraction of active PSII during extended periods of cell growth. The failed recovery in the fraction of inactive centers appears to a reversible mis-assembly involving the accumulation of photooxidized, but non-catalytic high valence Mn at the donor side of photosystem II, and that a reductive mechanism exists for restoration of assembly capacity at sites incurring mis-assembly. Given the established role of Ca^{2+} in preventing misassembled Mn, we conclude that D1-E189K mutant impairs the ligation of Ca^{2+} at its effector site in all PSII centers that consequently leads to the mis-assembly resulting in accumulation of non-catalytic Mn at the donor side of PSII. Our data indicate that D1-E189 is not functionally involved in Mn^{2+} oxidation\binding at the HAS but rather involved in Ca^{2+} ligation and steps following the initial Mn^{2+} photooxidation.

Keywords: Photosynthesis, photosystem II, dark rearrangement, calcium

1. Introduction

The photosystem II (PSII) reaction center complex of photosynthetic organisms catalyzes the extraction of electrons from water molecules to plastoquinone, harnessing light as the energy source to drive this highly endergonic electron transfer. Primary charge separation in PSII involves the formation of the highly oxidized electron donor P_{680}^{+} and a pheophytin within the D1/D2 polypeptide core buried within the large PSII complex. P_{680}^{+} is a powerful oxidant capable of extracting the electrons from the H_2O-oxidizing Mn_4O_5Ca metal cluster via a neighboring redox active tyrosine residue (Y_Z) of the D1 protein (1, 2). After each charge separation, the Mn cluster advances from a more reduced to a more oxidized state, with every state corresponding to one of the five so-called storage states (S_0, S_1, S_2, S_3, and S_4) of S-cycle. The oxidation of two H_2O molecules H_2O with the release of molecular oxygen is triggered by the formation of S_4 state, which is rapidly reduced by the substrate H_2O to the S_0 state, representing Mn cluster ground state (3).

The assembly of the Mn_4O_5Ca metal cluster within the protein matrix of the water oxidizing complex (WOC) is termed as photoactivation. It is an oxidative process that stepwise incorporates Mn^{2+} into the high valent $Mn^{\geq 3+}$ oxo-bridged structure that characterizes the H_2O-oxidation catalyst. Importantly, the first two Mn^{2+} oxidation events are separated by a poorly understood rate-limiting light independent process termed as dark rearrangement, k_A (Scheme 1).

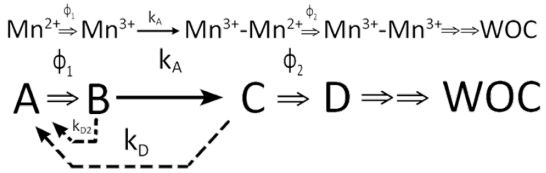

Scheme 1. Kinetic scheme of basic two-quantum mechanism of PSII photoactivation. Double arrows indicate light-activated processes with the quantum efficiencies $\boldsymbol{\phi}_1$ and $\boldsymbol{\phi}_2$ representing the first and second photooxidative events in the assembly sequence, k_A representing the "dark" rearrangement, and k_D, representing the decay of intermediates. After the initial two Mn are photoligated, subsequent Mn appear to be added with high quantum yield.

Remarkably, photoactivation utilizes essentially the same redox active cofactors as the regular electron transfer pathway during H_2O-oxidation catalysis. It begins with photochemical charge separation with the D1/D2 reaction center core with the formation of the highly oxidizing P_{680}^{+} species. During assembly, P_{680}^{+} extracts electrons, again via Y_z, from Mn^{2+} ions that diffuse from the soluble phase and bind within the apo-WOC at the so-called high affinity site (HAS). These Mn^{2+} ions successively become photooxidatively incorporated into the growing metal cluster [reviewed in (4)]. Current evidence suggests that Mn^{2+} photooxidation corresponds to the formation of a Mn^{2+} hydroxide intermediate at the HAS (5, 6). The exact location of the HAS is still a matter of debate. Surveys of amino acids at the PSII donor side using site-directed mutagenesis revealed D1-Asp170 is most important for the high affinity Mn^{2+} binding and photooxidation in apo-PSII (7-11). Not surprisingly, the affinity for Mn^{2+} ions ($K_M < 10$ μM) at the HAS

81 (5, 8, 12) has strong pH dependence, highlighting with the importance of the protonation state of the amino
82 acid residues coordinating Mn^{2+} and the likely hydroxide form of the bound Mn^{2+} prior to photooxidation
83 (5). In the crystal structure of the fully assembled complex, D1-Asp170 provides one of two oppositely
84 arranged axial monodentate carboxyl ligands of the so-called dangler Mn (Mn4) in intact WOC.
85 Interestingly, the other ligand, D1-Glu333, does not seem to be directly involved in the formation of the
86 HAS of apo-PSII, although it weakly influences the affinity of Mn^{2+} at the HAS (11, 13, 14). The evidence
87 that D1-Glu333 does not partake in the formation of the HAS is consistent with recent cryo-EM structures
88 of apo-PSII revealing that the carboxyl domain of the D1 protein adopts a very different conformation and
89 with several residues, including D1-Glu333, are shifted several Ångstroms away from their final positions
90 in the assembled complex (15, 16). The absence of direct Mn coordination by D1-Glu333 is interesting in
91 the light of the assumption that the high affinity binding of Mn^{2+} ion requires two carboxylate moieties (17).
92 Interestingly, D1-His332 is slightly shifted towards hypothetical HAS in apo-PSII and could be involved
93 in coordination of the Mn^{2+} ion (15, 16). The closest carboxylate moiety in apo-PSII to D1-Asp170 is D1-
94 Glu189, which occupies a similar position (1.1 Å difference relative to the assembled structure) in the
95 presence and absence of the Mn cluster. The distance between D1-Glu189 and D1-Asp170 in apo-PSII is
96 ~6.0 Å, which is in agreement with the distances found in mature PSII between carboxylate and intervening
97 Mn ions and, on this basis, has been proposed that D1-Glu189 and D1-Asp170 participate in the formation
98 of the HAS, perhaps in conjunction with D1-His332 (15, 16). Importantly, the most recent cryo-EM
99 structures (16) of apo-PSII reveal an unidentified a heavy atom, probably either Mn or Ca, located midway
100 between the carboxylate moieties of D1-Glu189 and D1-Asp170. This precise spatial arrangement is not
101 found in the assembled complex since these residues are slightly shifted in orientation compared to their
102 assembled configuration and the heavy atom appears to be in slightly different place than any of the metal
103 ions of the assembled Mn_4O_5Ca. The D1-Glu189 and D1-Asp170 residues share another important
104 characteristic, at least in the assembled complex: besides providing monodentate coordination to Mn (Mn1
105 and Mn4, respectively), their carboxylate groups each provide a second monodentate ligand to the sole Ca
106 ion of the Mn_4O_5Ca (14). In this context, the photoactivation of the Mn_4O_5Ca requires the presence of Ca^{2+}
107 during the assembly process and without Ca^{2+}, inactive high valent Mn accumulates (18).

108 Besides providing a ligand to Mn1, D1-Glu189 modulates the redox properties of Y_Z in addition to
109 those of the Mn cluster (19, 20). Additionally, D1-Glu189 is involved in the formation of a H-bonding
110 network, potentially accepting a proton from D1-His190 (21, 22). Most of the D1-Glu189 site-directed
111 mutants assemble partial or complete Mn clusters, possibly having defects in cluster assembly (19, 23).
112 Most of these mutants have lost the ability to evolve oxygen, despite containing photooxidizable Mn *in vivo*
113 (19). Recent time-resolved X-ray crystallography indicates that D1-Glu189 side chain moves away a from
114 the Mn_4O_5Ca during the S_2-S_3 transition, such that the ligand to the Ca ion is broken, but the D1-Glu189-

115 Mn1 ligation is maintained (24, 25). This movement appears to facilitate the Ca^{2+}-mediated insertion of
116 substrate H_2O between Mn1 and the Ca, thereby producing the O_x (O_6) proposed to be one of the two
117 oxygen atoms of the O_2 formed in the final stages of water oxidation (25-28). On the other hand, the fact
118 that several mutations with disparate chemical properties can substitute for glutamate suggests this role is
119 not decisive in the catalytic mechanism.

120 Given recent results indicating that the D1-Glu189 is potentially involved in the formation of the HAS
121 of PSII, we studied the photoactivation characteristics of three site directed mutants with lysine, arginine
122 and glutamine substitutions at the 189 position of D1 protein, which are substitutions that permit relatively
123 high rates of oxygen evolution (19), yet are shown to alter the assembly if the Mn_4O_5Ca.

124 2. Materials and Methods

125 2.1. Strains and Growth Conditions.

126 The glucose-tolerant strain of *Synechocystis sp.* PCC6803 GT (hereafter *Synechocystis*) (29) served
127 as the basis for all strains conducted in this study. The wild-type control strain (WT control) was constructed
128 by transforming strain 4E3 HT-3 returning the wild-type *psbA2* gene to its native location and with its
129 native promoter using *psbA2* using in the suicide plasmid pRD1031 as described previously (30). The 4E3
130 HT-3 strain lacks all three *psbA* genes and has the CP47 gene hexahistadine tag at its carboxy terminus.
131 Transformation of 4E3 HT-3 with the wild-type *psbA2* gene restored wild-type levels of D1 expression and
132 oxygen evolution under normal growth conditions (30). Site-directed mutations in the *psbA2* gene encoding
133 the D1-E189Q, D1-E189K and D1-E189R amino acid substitutions involved similar transformations, but
134 using site-directed mutant *psbA2* alleles resulting the mutant strains (31). All *Synechocystis* strains were
135 routinely maintained on BG-11 agar plates with addition of 10 µM DCMU and 5mM glucose as described
136 previously, to prevent reversion and suppressor mutations since these conditions remove any selective
137 advantage higher PSII activity (32). Experimental cultures were grown in 1 L flat flasks in 800 mL of BG-
138 11 with the addition of 10 mM HEPES-NaOH pH 8.0 and 5mM glucose under PFD (photon flux density)
139 of ~100 µmol m^{-2} s^{-1} at 30 ˚C. Light intensity was measured with Walz light meter (Germany). All
140 experimental cultures were harvested in late log phase (O.D. 750nm ~1.2-1.5) and checking the variable
141 fluorescence (F_V) value maximal for every strain (supplementary Table 1) as determined with a PSI
142 fluorometer (PSI instruments) using $F_v = (F_{max} – F_0)/ F_0$.

143 2.2. Hydroxylamine Extraction of Cells.

144 Cultures were centrifuged in 1 L bottles at 6000g (Sorvall, F9 rotor) for 12 minutes at room
145 temperature. Extraction of the Mn_4O_5Ca using hydroxylamine (HA) was performed as described previously
146 (33, 34). Briefly, cells were washed in BG-11 and concentrated to a chlorophyll concentration of 100 µg/mL,

HA was added to a cell suspension from a 400 mM freshly prepared stock to a final concentration of 10mM (35). Cell suspension was incubated in the dark on a rotary shaker at ~120 rpm at room temperature for 12 minutes. After the incubation, cells were diluted with 5x volume of BG-11 and centrifuged at 10200g (Sorvall, F14 rotor) at room temperature for 5 minutes. This washing step was repeated for 7 more times. After the washing was complete, cells were resuspended to [Chl] of 100 µg/mL and kept in the dark with shaking at ~120 rpm.

2.3. Photoactivation of HA-Extracted cells.

HA-extracted were either photoactivated using single-turnover Xenon lamp flashes or continuous light (Cool White fluorescent) at an intensity of ~50 µmol m^{-2} s^{-1}. Single-turnover Xenon lamp flash illumination was carried out as described previously in (34). A 400 µL aliquot of cells containing ~40 µg of chlorophyll was taken from the cell suspension kept in the dark. Cells were placed on a sample vessel fashioned out of an aluminum weighing cup with the stirring bar and covered with yellow UV filter to minimize UV damage to the sample. The sample was subjected to saturating single-turnover Xe flashes to promote photoactivation. Saturation of samples by Xe flashes was ensured by pre-tests using neutral density filters. Flash illumination was followed by the measurement of light-saturated rates of O_2 evolution to evaluate restoration of catalytic activity. To accomplish this, aliquots containing 10 µg of Chl were withdrawn from the photoactivated cell suspension and placed in the Clark-type electrode (Yellow Springs Instruments) chamber containing buffered BG-11 with the addition of 1mM DCBQ and 1mM potassium ferricyanide. The oxygen evolution rate was measured in response to saturating orange light (>570 nm) at 30˚C.

2.4. Curve fitting and data analysis.

Experiments measuring the photoactivation of the Mn-depleted PSII as a function of single-turnover flashes and a function of the flash interval allowed us to evaluate both the quantum efficiency of photoactivation and to estimate the kinetic parameters for the dark rearrangement and decay of intermediates (36). The rate constants for the dark rearrangement, k_A, and the decay of intermediates, k_D, were determined by deriving kinetic parameters from the rising and falling slopes of the bell-shaped curve in plots of photoactivation as a function of the flash interval curve fitted to the equation (35, 37-39):

$$[A]_n = [A]_0 \times (1 - e^{-\Phi_{PA1}\mathrm{n}}) \times (e^{\Phi_{PA2}\mathrm{n}}) \qquad \text{Equation 1}$$

Where $[A]_n$ represents the yield of active centers on the *n*th flash, $[A]_0$ is the concentration of apo-PSII centers prior to the photoactivation, $\boldsymbol{\Phi}_{PA1}$, and $\boldsymbol{\Phi}_{PA2}$ represent two apparent phases of photoactivation: a more efficient phase most obvious in the beginning of the flash sequence and lower efficiency phase afterwards.

$$[A]_n = [k_A/k_D - k_A] \times [A]_O \times \left(e^{-k_A td} - e^{-k_D td}\right). \quad \text{Equation 2}$$

Where k_A and k_D represents for the dark rearrangement and the decay of intermediates, respectively.

2.5. Fluorescence relaxation kinetics.

Flash-induced fluorescence yield relaxation kinetics was measured as described by Vass and coworkers (40) using FL-3300 fluorometer (PSI Instruments, Czech Republic). The duration of actinic and measuring light pulses were 30 µs and 9 µs, respectively, and relaxation of fluorescence yield was measured from range of 100 µs to 100 s. Samples were diluted to a concentration of 5 µg of Chl/mL in 3 mL of BG-11 and placed into the 4-sided clear cuvette for measurement. Multi component fluorescence relaxation analysis was performed as earlier by Vass (40, 41) by using fitting function with two or three components:

Table 1. Multicomponent kinetic equations used to fit the data from the data plots obtained from fluorescence relaxation kinetics experiments.

Components	Equation
Fast – Exponential Middle – Exponential Slow – Hyperbolic	$F(t) - F_0 = A_1 \exp\left(-\frac{t}{T_1}\right) + A_2 \exp\left(-\frac{t}{T_2}\right) + A_3/(1 + \frac{t}{T_3})$
Fast – Exponential Slow – Hyperbolic	$F(t) - F_0 = A_1 \exp\left(-\frac{t}{T_1}\right) + +A_2/(1 + \frac{t}{T_2})$
Fast – Exponential Middle – Hyperbolic Slow – Hyperbolic	$F(t) - F_0 = A_1 \exp\left(-\frac{t}{T_1}\right) + A_2/(1 + \frac{t}{T_2}) + A_3/(1 + \frac{t}{T_3})$

Where $F(t) - F_0$ is relative fluorescence yield, A_1-A_3 are decay amplitudes, T_1-T_3 are time constants from which the half-times can be calculated via $t_{1/2} = \ln 2\ T$ for exponential components and $t_{1/2}$ = is T for hyperbolic component.

3. Results

3.1. Photoactivation in continuous light shows altered Mn_4O_5Ca assembly in mutants.

There is consensus that D1-Asp170 is critical for the binding and photooxidation of Mn^{2+} at the HAS (7, 8, 11, 35), consistent with it providing a monodentate ligand to Mn4 in the assembled complex (14). However, recent cryo-EM studies of Mn-depleted PSII and PSII assembly intermediates that lack the Mn_4O_5Ca indicate the HAS is structurally quite different in the apo-PSII and identify two additional residues potentially involved in the formation of the HAS in apo-PSII and thus potentially involved in photoactivation. These residues, D1-Glu189 and D1-His332, are shifted towards the D1-Asp170 side chain compared to mature PSII. Their close proximity to D1-Asp170 potentially allows for Mn^{2+} to be coordinated between them, which is in accord with the observation of an unidentified heavy atom located midway between the D1-Asp170 and D1-Glu189 carboxyl groups (15, 16). To test the general hypothesis that D1-Glu189 modulates photoactivation, two amino acid substitution mutants capable of relatively high rates of oxygen evolution, D1-E189Q, D1-E189K and D1-E189R (**Supplementary material**) were

206 investigated. In addition, the D1-D170E mutant, which was previously shown to have a lower quantum
207 efficiency of photoactivation (35) was also included in this study for comparison.

208 The oxygen evolution rates in freshly isolated cells are shown in Figure 1A. The site-directed
209 mutants exhibit rates that are approximately 60% of the WT control, with the exception of D1-E189K which
210 was about 80% (19). The results confirm the initial studies on these mutants and demonstrate that even
211 relatively drastic amino acid substitutions such as D1-E189K still allow the assembly of active PSII under
212 the protracted conditions of growth and that the assembled Mn_4O_5Ca has robust H_2O-oxidation activity
213 despite the mutations. To gain information on whether the mutations affect the kinetics of assembly, cells
214 were treated with hydroxylamine to remove active Mn and samples were photoactivated under continuous
215 light (**Fig. 1B**). The extent of recovered O_2 evolution activity is expressed as a ratio of the recovered rate to
216 the rate prior to HA-extraction. Consistent with previous results, WT control cells recovered >90% of their
217 original activity within 15 min of illumination. Photoactivation of HA-extracted D1-D170E cells restored
218 approximately 70% of the original activity, but this took longer, ~40 minutes. This consistent with the flash
219 experiments (next section) and previous findings (35) showing reduced quantum efficiency of
220 photoactivation. Thus, substitution of Asp170 of the HAS, with the slightly large Glu side chain, permits
221 assembly, but with reduced quantum efficiency. Consistent with the nature of the amino acid substitutions,
222 the restoration of the O_2 activity was dramatically different D1-E189K and D1-E189Q mutants: D1-E189Q
223 was able to show similar restoration level to D1-D170E. However, it required only 20 minutes to reach
224 70% of its initial activity, while D1-E189K with the highest net O_2 evolution activity restored only 40%
225 even after 40 minutes of illumination respectively. Such low level of restoration in D1-E189K despites the
226 relatively high extent of assembly possible when grown in culture.

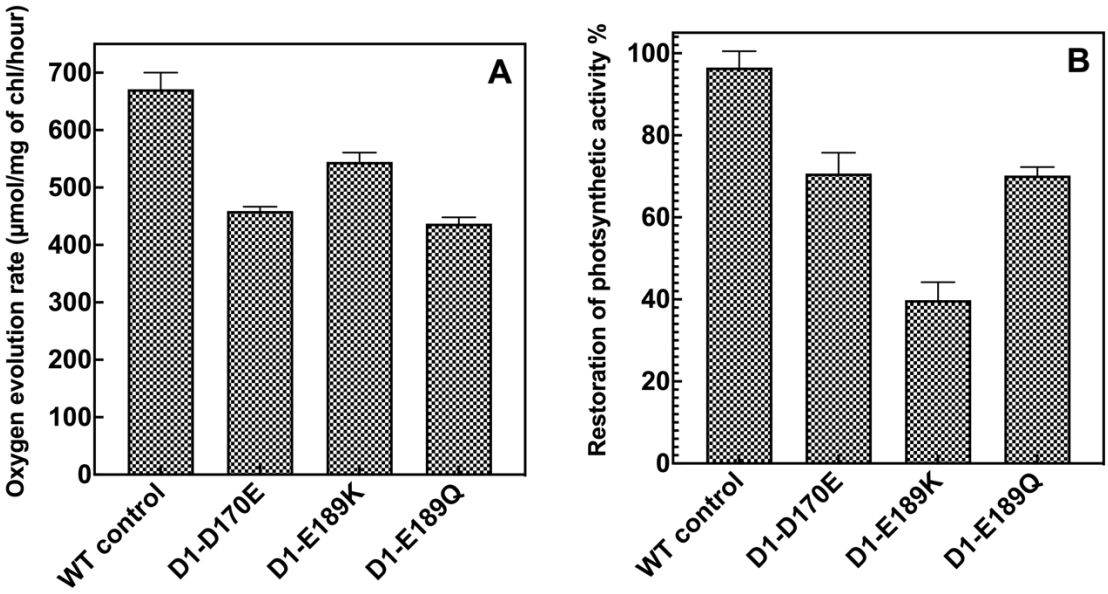

227

228 **Figure 1.** Light-saturated O_2-evolution activity of *Synechocystis* cells (A) harvested directly from growth culture. (B)
229 Recovery of light-saturated O_2-evolution activity of HA-treated *Synechocystis* cells after photoactivation under
230 continuous illumination. HA-treated cells were exposed to continuous illumination (~20 µmol m^{-2} s^{-1} PD) while being
231 gently shaken. Oxygen evolution activity was measured using a Clark-type electrode in HN buffer (10mM HEPES,
232 30mM NaCl, pH 7.2 in the presence of 1mM DCBQ and 1mM potassium ferricyanide). Oxygen evolution was
233 measures in response to saturating (>570 nm) illumination at 30˚C. The original light-saturated O_2-evolution rates
234 prior HA extraction were 671 ± 29, 459 ± 7, 544 ± 16, and 437 ± 11 µmol of O_2 (mg Chl)$^{-1}$ h^{-1}, for WT control, D1-
235 D170E, D1-E189K and D1-E189Q respectively. Error bars represent SD with n ≥ 3.

236 ## 3.2. Restoration of the O_2 evolving activity

237 The photoactivation as a function of the number (**Fig. 2**) and frequency (**Supplementary results**)
238 of saturating, single-turnover Xe flashes allows us to gather the values of quantum efficiency of
239 photoactivation i.e., estimate values that reflect the per flash development of O_2 evolution activity in Mn-
240 depleted samples and estimate the stability of the intermediates formed during the photoactivation.

241 The yields of photoactivation as a function of flash number are illustrated in Figure 2. For this
242 experiment, the uniform flash interval of 500ms (2 Hz) was used to photoactivate the samples. Consistent
243 with the previous results (34, 35, 42), HA-treated WT control cells reached approximately 85-90% if initial
244 activity after 2000 flashes, while 6400 flashes resulted in almost complete restoration of O_2 activity (**Fig**
245 **2**). The D1-E189Q mutant exhibits similarly shaped photoactivation curve as the WT control, however it
246 never approaches complete photoactivation. The maximum restoration of O_2 activity of 80% was observed
247 after 2000 single-turnover flashes and percent activity does not significantly increase even after 6400
248 flashes. This behavior contrasts with both WT-control, which is capable of reaching nearly 100% of initial
249 activity, and D1-D170E mutant that exhibits lower quantum efficiency of photoactivation but nevertheless
250 continues to develop O_2 evolution rate throughout the entire series of photoactivation flashes although not
251 reaching levels as high as the WT even after 6400 flashes. Unlike D1-E189Q, D1-E189K caused a severe
252 inhibition of photoactivation under flash illumination (**Figs. 1B, 2**) even though the maximal O_2 net rates
253 prior to extraction being similar to the other mutants (**Fig 1A**). A series of 2000 photoactivation flashes
254 given to D1-E189K mutants resulted only in 40% interestingly, the level of photoactivation shows little
255 increase even after 6400 flashes.

256 To derive the constants of both high and low efficiency phases of photoactivation seen in **Fig 2**, the
257 obtained data was fit into the double exponent equation 1. The quantum efficiency of the photoactivation,
258 $\boldsymbol{\Phi}_{PA1,2}$ (**Table 2**), in all studied mutants indicates the severe effect of the mutations at the HAS on the overall
259 efficiency of the light driven assembly of the Mn_4O_5Ca cluster but distributed differently between the two
260 phases. Interestingly D1-D170E mutant, which is shown to have a significantly lower quantum efficiency
261 of photoactivation is capable of high levels of restoration. Although D1-E189K show higher $\boldsymbol{\Phi}_{PA1}$ than D1-
262 D170E, it fails to reassemble Mn cluster in the majority of the PSII centers indicating on an irreversible
263 inhibition of the photoactivation. All of the studied D1-E189 mutants share a similar feature of an efficient

initial photoactivation phase within first 400-800 flashes followed by a significant decrease in the efficiency in assembly and failure to restore activity in a large fraction of centers.

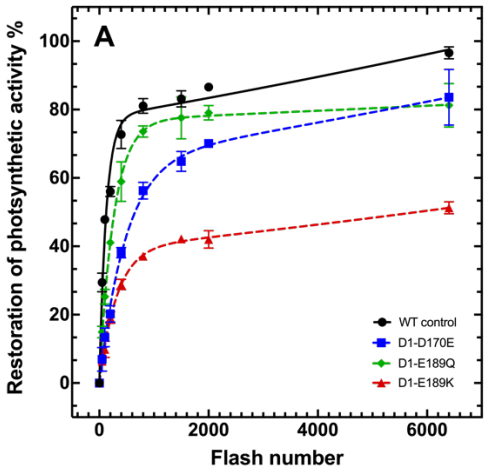

Figure 2. Photoactivation of HA-extracted cells as a function of the single-turnover flash number**.** Series of xenon lamp flashes were given at uniform frequency of 2 Hz (500ms flash interval) to hydroxylamine-treated WT control, D1-D170E, D1-E189Q, D1-E189K,. The percentage of O_2 evolution recovery was calculated as a fraction from the O_2 evolution rate prior HA extraction as described in Figure 1. Error bars represent SD with $n \geq 3$.

Table 2. Quantum efficiency of photoactivation of WT control, D1-D170E, D1-E189K and D1-E189Q mutant strains. Kinetic fit parameters of $\boldsymbol{\Phi}_{PA1}$ *and* $\boldsymbol{\Phi}_{PA2}$ obtained from the data from the plots in Figure 2 was fit into Equation 1.

Strain	Quantum efficiency of Photoactivation, Φ_{PA1}	Quantum efficiency Restoration, Φ_{PA2}	R
WT control	8.1×10^{-3}	3.6×10^{-5}	0.98
D1-D170E	2.1×10^{-3}	3.8×10^{-5}	0.99
D1-E189K	3.2×10^{-3}	4.2×10^{-5}	0.99
D1-E189Q	3.8×10^{-3}	9.1×10^{-6}	0.99

3.3. Mutations at D1-E189 does not alter the affinity at the HAS

Among the studied D1-E189 site directed mutants, D1-E189K represents greater interest due to the intriguing relationship between high net oxygen evolution activity (**Fig. 1A**), an impaired ability for *de novo* assembly of the Mn_4CaO_5 cluster (**Figs. 1B and 2**), and no apparent changes to the dark rearrangement and stability of photoactivation intermediates (**Fig. S1, Table S2**). While the photoactivation experiments fail to explain intriguing behavior of D1-E189 mutants, fluorescence relaxation kinetics experiments (**Supplementary results**) potentially indicate on a lower Mn^{2+} binding affinity at the HAS (**Fig S2, Table S2**). To estimate the effect of the lysin substitution on the Mn^{2+} binding at the HAS during photoactivation, the electron donation from Mn^{2+} to Y_z was measured in highly purified Mn-depleted PSII core complexes

283 as a function variable fluorescence (43). Mn^{2+} binding constant at the HAS in Mn-depleted PSII was earlier
284 estimated at approximately 1μM and has been shown to be strong pH dependent (5, 8, 44, 45) (46). When
285 the first charge separation occur, the redox-active Y_z re-reduces a primary chlorophyll donor, P_{680}^+. At the
286 time of the second charge separation in the Mn-depleted PSII, Y_z is already in the oxidized state and in the
287 absence of electron donor it is unable to re-reduce P_{680}^+, which results in the strong variable fluorescence
288 quenching by meta-stable P_{680}^+. In the absence of Mn^{2+} bound at the HAS, second and subsequent charge
289 separations result in essentially complete fluorescence quenching, however binding of Mn^{2+} at the HAS can
290 completely restores electron transport, yielding high fluorescence after each flash (5, 43, 47).

291 The electron flow from Mn^{2+} to Y_Z has a strong [Mn^{2+}] dependence (**Fig. S4, Table 4**), at very low
292 Mn^{2+} concentrations (<1μM) Y_Z is not able to re-reduce the entire population of P_{680}^+ resulting in
293 fluorescence quenching, however at K_m and saturating [Mn^{2+}] the reduction of P_{680}^+ produce a high
294 fluorescence yield allowing to estimate the binding affinity of Mn^{2+} at the HAS as a function of variable
295 fluorescence. Consistent with the previous findings (5, 8, 44, 45) (46), the value for Mn^{2+} dissociation
296 constant at the HAS in WT control Mn-depleted PSII complexes was shown to be at ~2.2 μM. Surprisingly,
297 the K_m value for D1-E189K at physiological pH 6.0 appeared to be only slightly different from WT
298 dissociation constant, ~2.9 μM indicating that Mn^{2+} binding at the HAS and consequent electron donation
299 is not impaired in this mutant. If the affinity change at pH 6.0 would be the sole reason for D1-E189K
300 inability to assemble the a large fraction of center we would expect the kinetics similar to D1-D170E mutant
301 (**Fig. 2**), however it seems that slightly lower K_M at pH 6.0 could be only accounted for the decreased
302 quantum efficiency of photoactivation during the early phase in D1-E189K mutant (**Fig. 2, Table 2**). On
303 the opposite, Mn^{2+} affinity in D1-D170A (**Fig. S4, Table 4**), that has been shown to have a drastic effect
304 on Mn^{2+} affinity at the HAS and fail to grow photoautotrophically (8), was previously estimated at ~50 μM
305 Mn^{2+} possibly indicating on a dominant role of D1-D170 in the formation of the HAS in a comparison to
306 D1-E189.

307 Lysin possesses one of the highest side chain's pKa values among all standard amino acids, for the
308 sake of the current experiment the assay buffer pH was also set to pH 7.5. At elevated pH the affinity at the
309 HAS in WT and D1-E189K was essentially the same again suggesting that D1-E189K is not involved in
310 initial Mn^{2+} binding and oxidation at the HAS.

Mn^{2+} affinity, μM		
Strain	**pH 6.0**	**pH 7.5**
WT control	2.2	1.1
D1-E189K	2.9	0.9
D1-D170A	50*	28.9

311 **Table 4.** Mn affinity at the HAS in purified Mn-depleted PSII from WT control, D1-E189K and D1-D170A. Obtained
312 values were derived from the fluorescence plots fitted into Michaelis-Menten equation (**Fig. S4**) and based on Mn^{2+}
313 electron donation capabilities in studied mutants. * Km value adapted from Nixon and Diner, 1992 (8)

314 3.4. Accumulation of unstable photooxidant at the donor side of PSII

315 The observation that D1-E189K mutant has no small changes in Mn^{2+} affinity at the HAS (**Fig. S4,**
316 **Table 4**) but yet reach only 40% of maximal O_2 evolution activity after treatment with hydroxylamine (**Fig.**
317 **1B**) combined with the biphasicity of the assembly process (**Fig. 2**) may indicate on a 'bifurcation' of the
318 photoactivation process with essentially two population of centers being formed, active and inactive.
319 Previous analysis concluded that these mutations in this position result in cells containing both intact
320 catalytic Mn clusters, plus significant fractions inactive centers containing photooxidizable Mn (19). To
321 investigate if the mutations at the HAS indeed result in the formation of photooxidant at the donor site of
322 apo-PSII (40, 41) we sought to partially photoactivate the cells to approximately 20-30% of maximal
323 restoration level (**Fig. 2**) with 50 and 200 flashes for WT and D1-E189K respectively and estimate the
324 stability of the photooxidant after the dark incubation. In the D1-A344Stop mutant, which fails to assemble
325 active Mn_4O_5Ca centers, charge separation induces the formation of unstable photooxidized $Mn^{\geq+3}$ capable
326 of serving as an oxidant of Q_A^- and resulting in characteristic changes in Chl fluorescence relaxation kinetics
327 with an increase in the proportion of fluorescence relaxation occurring more slowly ($t_{1/2}$~ 240ms). Moreover,
328 dark incubation resulted in the loss of non-functional $Mn^{\geq+3}$ (41).

329 Similarly, the purpose of the dark incubation (40 min) in the present experiments with partially
330 photoactivated cells is to allow the re-reduction of unstable photooxidized Mn at the donor side, which
331 might alter fluorescence relaxation kinetics (**Fig. S2, Table S2**). After the partial photoactivation WT
332 control showed the reduction of the decay yield during the slow phase (55%) and appearance of the middle
333 phase (1s, 27.4%) (**Fig. 4A**). The dark incubation of WT control cells has not significantly changed
334 fluorescence relaxation kinetics indicating that the majority of photooxidized Mn at the donor side is
335 assembled into functional and stable Mn cluster (**Fig. 4C**). Similarly to WT control, D1-E189Q mutant did
336 not exhibit any significant changes in the fluorescence relaxation kinetics after the dark incubation (**Fig. S5**
337 **B&E, Table S4**).

338 Photoactivation of D1-E189K (**Fig. 4B**) mutant with 200 flashes resulted in decreased time constant
339 for the slow phase (100 s, 31%) compared to HA-extracted cells (>100 s, 41%) and increased half time of
340 the middle phase from 144 ms and 18.5% to 457 ms and 27.6% of total yield respectively. Dark incubation
341 caused the decay of unstable photooxidant at the donor side of D1-E189K mutant with consequent increase
342 of the time constant and yield for the slow phase (>100 s, 44%) and decrease of the decay yield during the
343 middle phase (16.7%) (**Fig. 4D**). Similarly, D1-D170A and D1-E189R mutants showed noticeable changes
344 in the fluorescence relaxation after the dark incubation, indicating on a portion of unstable photooxidized

Mn accumulated at the donor side of PSII, however to a much smaller degree compared to D1-E189K mutant (**Fig. S5, Table S4**).

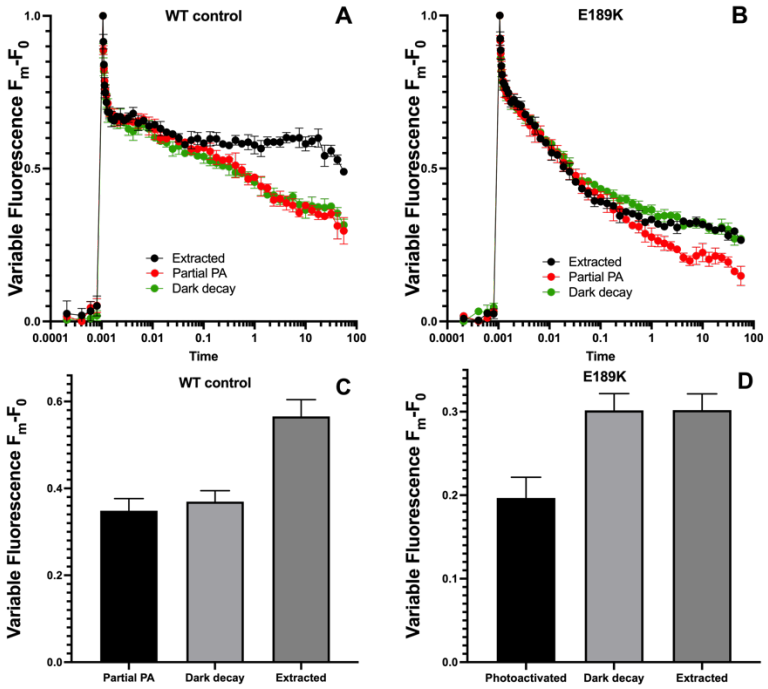

Figure 4. Q_A^- reoxidation kinetics in partially photoactivated **(A)** WT control and **(B)** D1-E189K in the presence of DCMU. For the purpose of the partial photoactivation the sequence of 50 and 200 single turnover flashes was given to the HA-extracted WT control and D1-E189K cells respectively at uniform interval at 2Hz (500ms flash interval). Dark incubated sample was stored in complete darkness on a rotary shaker for 40 minutes prior the measurements. Panels **(C)** and **(D)** show the relative difference in the fluorescence relaxation kinetics in WT control and D1-E189K prior photoactivation, after photoactivation and after the dark incubation, the average of the last 8 fluorescence datapoints from panels **(A)** and **(B)** were taken to obtain the bar plots, higher level of fluorescence after the dark incubation indicates on a slower relaxation due to the absence of electron acceptor at the donor side of PSII. The measurements were performed after a single actinic flash of light. Samples were dark adapted for 5 minutes prior the measurements. Error bars represent SD with $n \geq 3$

Table 5. Characteristics of chlorophyll fluorescence relaxation kinetics in partially photoactivated WT control and D1-E189K.

Partially photoactivated cells in the presence of DCMU					
Strain/State		**Fast phase: τ/ms (amplitude (%))**	**Middle phase: τ/ms (amplitude (%))**	**Slow phase: τ/s (amplitude (%))**	**R**
WT control	Extracted	7.9 (14.5)	(0)-	> 100 (85.4)	0.97
	Partial Photoactivation	8.5 (17.7)	1050 (27.4)	> 100 (54.9)	0.99
	Dark incubated	8.3 (19.9)	918 (22.3)	> 100 (57.9)	0.98
D1-E189K	Extracted	5.9 (40.5)	144 (18.5)	> 100 (40.9)	0.99
	Partial Photoactivation	7.4 (41.2)	457 (27.6)	100 (31.1)	0.99
	Dark incubated	7.9 (39.2)	440 (16.7)	> 100 (44.1)	0.99

For the purpose of the partial photoactivation the sequence of 50 and 200 single turnover flashes was given to the HA-extracted cells at uniform interval at 2Hz (500ms flash interval), respectively. The decay curves were analyzed by assuming exponential decay for the fast phase and hyperbolic for both middle and slow phases for D1-E189K, while for WT control exponential fit was used for the fast phase and hyperbolic for the slow phase (see Table 1).

4. Discussion

The primary event during light driven assembly of the Mn_4O_5Ca is the binding and photooxidation of a Mn^{2+} ion at the HAS of PSII (5, 6, 48). Previous mutagenesis studies (8, 23, 31, 35) identified D1-D170 as a key amino acid residue for Mn^{2+} binding and photooxidation, which represents the first step of photoactivation (**Scheme 1, A⇒B**). The crystal structure of holo-PSII reveals that the carboxyl group of D1-D170 provides one monodentate ligand to the 'dangler' Mn ion (Mn4) and one monodentate ligand the Ca^{2+} in the assembled complex. However, recent cryo-EM structures of apo-PSII show that this region of the WOC adopts a significantly different structural configuration compared to the fully assembled and active WOC (15, 16). Recently published apo-PSII structures identify electron density attributed to a heavy cation situated between the carboxylates of the D1-D170 and D1-E189, which was proposed to be an Mn^{2+} ion thus defining the HAS in apo-PSII. However, it is also possible that the observed density is a Ca^{2+}, a reasonable conclusion given that D1-E189 ligates Mn1 and Ca^{2+} in an intact Mn_4O_5Ca cluster. The site directed mutants at D1-D170 showed a dramatic effect of these mutation on the ability to bind and oxidize Mn^{2+} by apo-PSII (7, 31), which ranges from complete loss of the function in D1-D170A to mutants capable of assembling up to 50% of WT O_2 evolution activity in D1-D170E and D170H mutants (35). Less is known about the potential role of D1-E189 in forming the HAS, although early studies of D1-E189 mutants showed that many substitution mutants contain partially or misassembled Mn. Subsequent studies have shown that D1-E189 participates in a hydrogen bond network, modulates the redox potential of Y_Z, and undergoes a conformational movement during the catalytic cycle proposed to allow substrate water delivery to the active site. Despite these extensive studies in the framework of water oxidation (19-22), until now, there has not been an attempt to evaluate the potential role of D1-E189 in the formation of the HAS and the assembly of the Mn_4O_5Ca.

4.1. Does D1-E189 to help form the high affinity site of PSII?

The electron donation experiment (**Fig. S4, Table 4**) in D1-E189K shows that this mutant possess the same Mn^{2+} affinity at the HAS indicating on a correct formation of photoactivation intermediates **A** and **B**, while D1-D170 **(Table 4)** mutations at the HAS inhibit initial Mn^{2+} photooxidation (35), thus preventing the electron donation to P_{680}^{+} after the charge separation. Thus, analysis of the HAS characteristics of the D1-E189K, show that unlike mutations at D1-D170, the the Lys substitution of Glu189 does not affect the electron donation from Mn^{2+} towards Y_Z (**Fig. S4, Table 4**). Although a Lys substitution of D1-Asp170 has not been reported, the corresponding Arg mutation resulted in a five-fold reduction in affinity. Thus, we conclude that D1-E189 is not likely directly involved in forming the HAS. Consistent with previous results (19) D1-E189K mutation seems to have almost no effect on the O_2 evolution rate, which reaches up to 80% of WT control rate (**Fig. 1**). While D1-E189Q mutation decreases the maximal rate to a larger extent,

397 the net O_2 rates are still relatively high and reach approximately 60% (19). Despite significantly high O_2
398 rates in all studied D1-E189 mutants, an analysis of their photoactivation characteristics revealed severe
399 defects. While D1-E189Q was able to restore initial oxygen evolution activity up to 70% after 15 minutes
400 of continuous illumination, which is similar to the D1-D170E mutant. However, D1-D170E required twice
401 as much time to reach same level of restoration (**Fig. 1B**). The photoactivation in the D1-E189K mutant
402 was severely inhibited with the restoration level reaching 40% of initial O_2 evolution activity respectively
403 after 40 minutes of illumination. Unlike in the D1-D170E mutant where the $\boldsymbol{\Phi}_{PA1}$ was significantly lowered
404 (**Table 2**), D1-E189K, D1-E189Q and D1-E189R (**Supplementary materials**) mutants re-assemble the
405 Mn cluster at a much higher $\boldsymbol{\Phi}_{PA1}$ (**Fig. 2, Table 2**). However, after reaching 40% in D1-E189K and 80%
406 in D1-E189Q the photoactivation almost stops and continues with a relatively low $\boldsymbol{\Phi}_{PA2}$. Interestingly, D1-
407 E189R mutant show very similar photoactivation properties to D1-E189K, suggesting the similar inhibitory
408 role of positively charged amino acid on photoactivation (**Fig. S3**). The inability of the D1-E189 mutants
409 to restore high level of WOC activity could indicate on the presence of internal damage or inhibition
410 occurring either during the Mn-depletion procedure of photoactivation. Since all cyanobacterial strains were
411 essentially treated the same and neither WT control nor D1-D170E strains showed similar assembly
412 inhibition, it is unlikely that the treatment with 10mM of hydroxylamine caused the observed effect.
413 Moreover, photoactivation was similarly inhibited during preliminary Mn-depletion experiments with 2mM
414 of hydroxylamine in D1-E189K (**Fig. S6**). For all mutants the optimum interval between the photoactivation
415 flashes yielding the maximum recovery of oxygen evolution by WOC was observed at 200-500 ms range
416 (**Fig. S1, Table S1**), the flash interval experiments showed that the photoactivation intermediates in D1-
417 E189K decay faster than in the wild-type. However, neither the overall low quantum efficiencies of
418 photoactivation nor the increased rates of decay explain the inability of the D1-E189K to photoactivate
419 such a large proportion of centers. It is worth mentioning that D1-E189K mutant is showing significant
420 rates of O_2 evolution prior the HA-extraction (**Fig. 1A**), however not able to restore this activity rapidly
421 like WT control (**Fig. 1B**) while D1-E189Q similar to WT control is capable of rapid restoration of 80% of
422 the net O_2 rate (**Figs. 1B, 2**).

423 Analysis of the course of photoactivation under flash illumination revealed essentially two phases
424 of the restoration curve. One phase, the main phase, corresponds to relatively high quantum efficiency of
425 photoactivation, whereas the other phase involves a much lower quantum efficiency that, according to
426 previous *in vitro* studies (37), can actually be a negative indicator of damage to the reaction centers during
427 assembly. In the whole cell experiments conducted here, the main assembly phase in all mutants showed
428 decreased quantum efficiency, $\boldsymbol{\Phi}_{PA1}$ (**Table 2**) suggesting that D1-E189 is important during initial steps of
429 photoactivation. The reduced quantum efficiency, can be attributed to alterations in the HAS however,

again these alterations does not explain the inability of D-E189 mutants to photoactivate with the constant rate similar to D1-D170E.

4.2. Does D1-E189 ligand participate in the binding of Ca^{2+}?

D1-E189K mutant showed high quantum efficiency, $\boldsymbol{\Phi}_{PA1}$ early in the photoactivation that yields 40% of initial activity (**Fig. 2**) followed by the slow restoration phase, $\boldsymbol{\Phi}_{PA2}$ (**Table 2**). The reasons behind the fact that assembly significantly slows after a rapid phase of photoactivation, $\boldsymbol{\Phi}_{PA1}$ are intriguing and could be explained by the assumption that only a small fraction of the centers from the entire population of PSII are actually assembling functional WOC, while the remaining PSII centers are inhibited or severely slowed in assembly. This is consistent with the observation that unextracted D1-E189K cells exhibit significantly higher O_2 evolution rate (80% of WT), indicating that a larger population of centers could assemble WOC over long period of time, which in turn indicates the reversible nature of observed inhibition. This and observation that D1-E189K can assemble a fraction of active WOC (**Figs. 2 and S1D**) at reasonably high quantum efficiency (**Table 2**) suggests that inability to assembly WOC by D1-E189K is not the result of a failure to photooxidize Mn^{2+} (**Fig. S4, Table 4**) or perform the dark rearrangement (Fig. **S1D**), but rather a result of inhibitory effect occuring over the course of illumination.

The change in the fluorescence relaxation kinetics in the presence of DCMU in Mn-depleted and partially photoactivated cells (**Fig. 4, S5**) indicate the accumulation of the photooxidant at the donor side of apo-PSII capable of charge recombination with Q_A^-. Considering the efficient photoactivation in WT and D1-E189Q cells (**Fig. 2**) there are no doubts that these strains accumulated functional WOC over the course of 50 and 100 flashes respectively. Although the charge recombination pathway also occurred after the partial photoactivation of D1-E189K and D1-D170E (**Fig. 4, S5**) mutants indicating the accumulation of the photooxidant, the nature of the photooxidant remains unclear. Consistent with altered quantum efficiency of photoactivation, $\boldsymbol{\Phi}_{PA1}$ (**Table 2**) due to the mutation at the HAS, aforementioned mutants could accumulate a population of oxidized carotenoids that slowly recombine with Q_A^- (49) (**Fig. 4, S2, S5, Table 5**). However, this hypothesis again does not explain why D1-E189K mutant is not capable of acquiring a substantial fraction of active WOC during photoactivation (**Figs. 1B, 2**). Moreover, the retention of variable fluorescence indicates that this is not due to damage to the photochemical reaction center.

Alternatively, the photooxidant accumulated at the donor side of apo-PSII could be attributed to mis-assembled photooxidized Mn as predicted earlier by Chu *et. al* (10, 23), Hwang *et.* al (35) and observed by Cser *et. al* in D1-A344stop mutant (35, 41). Considering that the quantum efficiency of photoactivation, $\boldsymbol{\Phi}_{PA1}$ in D1-E189K mutant in fact was less severely affected compared to D1-D170E mutant and no significant effect on Mn^{2+} affinity at the HAS in D1-E189K was observed (**Fig. S4, Table 4**), we tentatively assign the accumulated photooxidant at the donor side of apo-PSII to misassembled non-functional

463 photooxidized Mn. The assumption that D1-E189K mutant accumulate non-functional Mn at the donor side
464 in the majority of centers would explain the inability of this mutant to restore a large fraction of active
465 WOC during relatively short course of photoactivation (**Figs. 1B and 2**). Although the mechanism of
466 inappropriate Mn accumulation is unclear, one hypothesis could be derived from the fact that besides Mn1,
467 D1-E189 coordinates Ca^{2+} in intact WOC (14). Considering the general agreement that Ca^{2+} is crucial for
468 photoactivation (12, 18, 37, 50) the actual mechanism how Ca^{2+} facilitates the photoassembly remains
469 elusive. Binding of Mn^{2+} to the HAS with simultaneous binding of Ca^{2+} to an adjacent binding site facilitates
470 the formation of the [Mn^{2+}-(OH)-Ca^{2+}] complex by inducing deprotonation of a water ligand of Mn^{2+}.
471 Calcium lowers the pK_a for water ligand, which is controlled by a nearby base B^- that serves as a primary
472 proton acceptor with a pK_a dependent on Ca^{2+} bound to its effector site (51). It is possible that D1-E189
473 ligand supports Ca^{2+} binding at its effector site in apo-PSII during early photoactivation steps. Considering
474 the strong competition between Mn^{2+} and Ca^{2+} for Ca effector site (37, 38) shown during *in vitro*
475 experiments, and the observed negative effect of D1-E189 mutations on the photoactivation it is reasonable
476 to assume that D1-E189K and potentially D1-E189R (**Fig. S3**) mutations could alter the binding of Ca^{2+} to
477 its effector site, thus even more increasing the Mn^{2+} inhibitory effect (37, 38). According to Chen *et al.* (18),
478 Ca^{2+} prevents inappropriate binding of high valency non-functional Mn ions at the donor side of apo-PSII
479 during the photoactivation, an effect that can also occur at high light intensities (43). Interestingly, partially
480 assembled Mn clusters were inferred by Cser and these appeared to be unstable in the dark, which resulted
481 in the loss of charge recombination pathways in D1-A344stop mutant (41). Consistent with earlier
482 observations, D1-E189K showed noticeable change in the fluorescence decay kinetics after partially
483 photoactivated samples were incubated in the dark (**Figs. 4B & D**), while WT (**Figs. 4A & C)** and D1-
484 E189Q (**Fig. S5**) strains have not shown any changes in fluorescence relaxation kinetics.

485 Assuming that in D1-E189K mutant only a fraction of the centers successfully ligated Ca^{2+} prior
486 the photoactivation, the entire population of centers undergo essentially two different pathways of
487 photoactivation. The bifurcation of the photoactivation process represent the ratio distribution of assembled
488 centers from the common pool of inactivated centers by hydroxylamine treatment and could be considered
489 a competition between productive photoactivation, when Ca^{2+} is bound at the effector site, and
490 nonproductive photoactivation in the absence of Ca^{2+}. The results observed during flash number
491 experiments in D1-E189K mutant indicate the ratio of non-functional Mn is much higher compared to WT
492 control and reaches up 60%, however D1-E189Q assembled approximately 80% of the centers correctly
493 and only smaller fraction of centers were inactivated (**Fig. 2**). The similarity in rate of the dark
494 rearrangement, K_A (**Table S1**), among the mutants suggests that the assembly of appropriate Mn cluster
495 occurs with similar kinetics, which in principle is not much different from WT control. The main difference
496 between these mutants is the distribution of the assembly pathways yielding different amounts of functional

497 and nonfunctional centers. Previous findings indicate that inappropriate Mn does not cause permanent
498 damage to the PSII centers and can be re-reduced by HA treatment allowing further photoassembly (35).
499 Our results show that D1-E189K reassemble non-functional Mn although at the slow rate (**Table 2**); that
500 would explain its ability to show high O_2 evolution rates prior the HA treatment.

501 4.3. Does the accumulation of non-functional Mn in PSII irreversibly inhibit 502 photoactivation?

503 As mentioned earlier the unique property of D1-E189K and D1-E189Q is a significant rate of
504 oxygen evolution among all PSII mutants. In principle this feature indicates that the cells are capable of
505 coping with the inhibition caused by the formation of non-functional Mn structures (35, 43) as discussed
506 earlier. However, it is not clear if non-functional Mn could be removed from the apo-PSII without the
507 initiation of PSII repair process, which involves the disassembly of PSII monomer and replacement of the
508 D1 protein (52-54). The evidence that the PSII centers populated with non-functional Mn at the WOC site
509 could be restored by hydroxylamine treatment (35) and by essentially the same electron donation capability
510 in D1-E189K (**Fig. S4, Table 4**) imply that the oxidative state of inhibitory Mn at the WOC most likely
511 higher than Mn^{2+} and that the reduction of such Mn results in its dissociation from the inhibition site.
512 Interestingly, in the absence of the PsbO protein, Mn_4O_5Ca cluster tends to be reduced in the dark, which
513 could result in complete loss of photosynthetic function in this mutant (42, 55). The fact that the ΔPsbO
514 mutant is capable of significant O_2 evolution suggests that the process of cluster reduction and re-assembly
515 happens concurrently under illumination. In principle, $\mathbf{\Phi}_{PA2}$ in D1-E189K and to a large extent in D1-E189R
516 (**Fig. S3**) mutant could indicate the reduction of 'wrong' Mn followed by new assembly trial over the course
517 of 6400 photoactivation flashes (**Fig. 2**). Since the Mn cluster in ΔPsbO can be reduced by endogenous
518 reductants in the lumen, non-functional Mn formed during the assembly in D1-E189K mutant could
519 potentially decay in the dark. Additional evidence for the reduction of partially assembled Mn cluster in the
520 dark come from D1-A344Stop mutant, where 40-minute dark incubation resulted in significant reduction
521 of the charge recombination between Q_A^- and photooxidized Mn at the donor side of PSII (41). Consistent
522 with these observations, the changes in fluorescence relaxation kinetics were not observed after the dark
523 incubation in WT control (**Fig. 4A & C**). The consistency in fluorescence decay kinetics prior to and after
524 the dark incubation indicate that the majority of assembled centers over the course of 50 flashes were
525 formed in fully functional and stable Mn clusters.

526 Among the studied strains only D1-E189Q mutant showed similar photoactivation to WT control
527 (**Figs. 2, S1**) and comparable Q_A^- reoxidation kinetics in the samples prior HA treatment and after Mn
528 extraction (**Fig. S2**). Similar to WT control, D1-E189Q exhibited virtually no difference in fluorescence
529 decay kinetics prior the dark incubation and after **(Figs. S4B & E)**. Despite the difference in pK_A between

530 Glu and Gln, D1-E189Q seems to be capable of supporting correct assembly of the Mn cluster similar to
531 WT control. Unlike in WT control and D1-E189Q strains **(Figs. 4, S5)** D1-E189K (**Fig. 4**) and D1-D170E
532 **(Figs. S5)** accumulated a portion of unstable photooxidant, that we assign to non-functional Mn, at the
533 donor site after the partial photoactivation. Similar to what has been observed in D1-A344Stop prior and
534 after the dark incubation, D1-D170E and D1-E189K mutants showed reduction in fluorescence decay rate
535 after 40-minute dark incubation (**Fig. S5, 4**). The slowdown in the fluorescence decay after the incubation
536 in the dark suggests that these mutants lost a fraction of redox active Mn involved in the charge
537 recombination between Q_A^- and the donor side of PSII. These observations support previous hypothesis that
538 during the photoactivation in D1-E189K mutant the assembly of the Mn cluster yields two types of centers,
539 active centers capable of water oxidation and non-functional but yet redox active centers containing at least
540 a single Mn^{3+} ion at the donor site of PSII (23). Importantly, the accumulation of the non-functional Mn by
541 D1-E189 mutants while retaining the fluorescence relaxation kinetics after the reduction of the non-
542 functional Mn indeed indicate on the absence of irreversible damage to the reaction centers similar to D1-
543 D170V mutant (35). The ability of this mutants to assemble up to 80% of active centers in regard to WT
544 control and the evidence that inappropriate Mn could be removed from the centers we suggest that the
545 formation of non-functional Mn clusters in D1-D170E and D1-E189K mutants is reversible and in a long
546 run does not prevent these mutants from assembling a significant portion of active PSII. However,
547 verification of the tentatively assigned "inappropriate Mn" (18), will require further *in vitro* studies with
548 purified PSII core complexes for careful investigation of the phenomenon.

549 5. Conclusions and model

550 In conclusion, while mutation of the D1-E189 ligand have a strong impact upon photoactivation,
551 this residue is not crucial for the formation of the HAS in assays monitoring Mn^{2+} binding and oxidation at
552 the HAS. Unlike most D1-D170 mutants (8), most of the D1-E189 mutants are capable in accumulation of
553 a large fraction (≥50%) of PSII centers containing photooxidazable Mn ions, although many of these are
554 not capable of oxygen evolution activity (19). Given that the D1-E189K mutant has very similar Mn^{2+}
555 affinity at the HAS, but is highly impaired in photoactivation, we conclude that the problems associated
556 with inability to assemble the Mn_4O_5Ca cluster in D1-E189K occur after the initial Mn^{2+} oxidation.
557 According to our model, D1-E189K plays a role in the formation of intermdediate '**C**' and/or the quantum
558 efficiency of the photoconversion of **C⇒D**, the step leading to the formation of a di-μ-oxo bridged binuclear
559 Mn^{3+}, proposed to be the first stable photoactivation intermediate and corresponding to the Mn(1) and
560 Mn(2) ion of the assembled cluster based upon experimental stability and calculated thermodynamic
561 grounds. We have earlier proposed the process leading to this state involved the translocation of the first
562 Mn^{3+} ion produced at the HAS (56). In the context of this translocation hypothesis, the present results

563 suggest the D1-E189 may help mediate this translocation. Given that D1-E189K does not perturb the
564 affinity of the HAS and observation of a cation situated between D1-Asp170 and D1-E189 in the apo-
565 structure, it may be that Ca^{2+} this position. It is worth noting that lysine substutions for carboxylates in the
566 Ca^{2+}-binding EF hand structure do not abolish Ca^{2+} binding, athough the affinity is diminished (57).
567 According to this model, the photoxidation of Mn^{2+} at the HAS with the presence of Ca^{2+} at an adjacent
568 binding D1-E189 site, facilitates the translocational rearrangement of the [Mn^{3+}-(OH)-Ca^{2+}] species
569 positioning the Mn^{3+} ion in a thermoduynamically more stable site corresponding to the Mn(1) and Mn(2)
570 locations in the intact PSII, which is consistent with results examining to location of photooxidized Mn ion
571 in PSII crystals that had been extracted and re-illuminated (58). The role of Ca^{2+} could be either: 1) blocking
572 the relocation of the newly formed Mn^{3+} ion into an inappropropriate site and/or 2) tethering and thereby
573 guiding the relocation into the correct site. Regardless, the relocation would open the HAS for the second
574 Mn^{2+} binding and photooxidation and and a similar repositioning of this second ion as it joins the first to
575 form the stable binuclear intermediate located at Mn(1) and Mn(2) and accompanied by protein structural
576 rearrangements involving the CP43 e-loop and the D1 c-terminus. Impairment of this Ca^{2+}-dependent
577 process would in this model leads to bifurcation of the photoactivation process resulting in essentially two
578 populations of centers, functional PSII, where Ca^{2+} was successfully bound for correct Mn^{3+} translocation
579 and PSII with photooxidizable Mn, where Ca^{2+} failed to mediate correct translocation and instead the ion
580 bindings to the Ca^{2+} site between D1-Asp170 and D1-E189. In this scenario, the subsequent Mn^{2+} oxidation
581 at the HAS initates the formation of non-catalytic Mn-oxide formation (59, 60).

582 # Supplementary results

583 ## 5.1. Dark molecular rearrangement and the stability of photoactivation
584 intermediates.

585 According to the "two-quantum model" of photoactivation (**Scheme 1**), the formation of the first stable
586 intermediate (intermediate **D**) involves two photoacts separated by a light-independent molecular rearrangement (4,
587 36). This rate-limiting rearrangement, combined with the limited stability of the photoactivation intermediates, results
588 in a bell-shaped curve when the formation of active PSII is promoted by a fixed number of flashes given at different
589 flash intervals, measuring the extent of recovery of O_2 evolution after the flash sequence (34, 35, 37, 39, 61).

590 For the present experiments, a fixed number of flashes, was determined for each strain to give approximately
591 50% recovery at optimal flash spacing. This number of flashes was given to HA-extracted samples at intervals ranging
592 from 50 millisecond to 10 seconds for each of the strains and the plotted yields at each flash frequency produced the
593 'bell-shaped' curves shown in Figure 3. To estimate time constants for the dark rearrangement, k_A, and the decay of
594 labile intermediates, k_D, the flash interval photoactivation data was fit into the equation derived from the two-quantum
595 model (35, 37, 39). The values for the dark rearrangement and the decay of intermediates in terms of half-times for
596 WT control were 66 ms and 1.8 s respectively (**Table 3**). All mutants studied showed similar moderately slowed
597 values for the dark rearrangement, k_A ranging from 78–82 ms, the rate-limiting, molecular rearrangement (**Scheme 1,**
598 **B→C**). Recent evidence suggests that the dark rearrangement, k_A, involves a conformational change of the metal-
599 binding polypeptide structure of the WOC (15, 37, 62). Since all mutants exhibit similarly decreased k_A value
600 compared to WT control, yet had markedly different extents of assembly, the reason behind the inability of D1-E189K

to assemble a large fraction of the PSII centers (**Figs. 1B and 2D**) is not associated with a slowed the rate of the molecular rearrangement (38, 42, 63, 64). Interestingly, all mutants exhibited decreased stability of the labile photoactivation intermediates (**Fig. 3, S1B and Table 3**). This result is consistent with D1-E189 providing as stabilizing interaction, either direct or indirect, with the Mn^{3+} ion produced during the initial photooxidation at the HAS **(A⇒B)**.

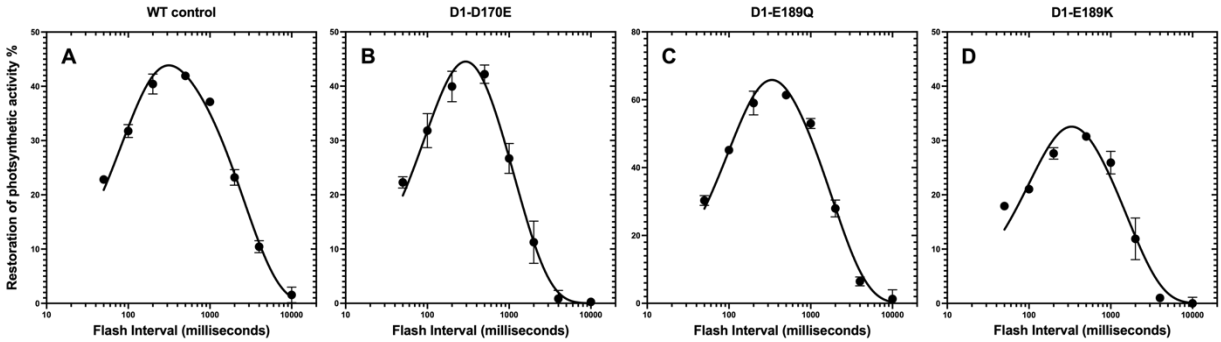

Figure S1. Photoactivation of HA-extracted cells as a function of flash interval. Flashes were given at six different equal flash intervals to HA-extracted WT control (Panel A), D1-D170E (Panel B), D1-E189Q (Panel C), D1-E189K (Panel D). The curves represent fits to Eq. 2 derived from the two-quantum model shown in Scheme 1 (39). The number of photoactivation flashes was determined based on the flash number experiment (Fig. 2) to produce approximately 50% restoration of activity. This corresponded to 150, 250, 350 and 500 for WT control, D1-E189Q, D1-E189K, and D1-D170E respectively. The percentage of O_2 evolution recovery was calculated as a fraction from the O_2 evolution rate prior HA extraction which were 600 ± 20, 369 ± 27, 520 ± 32 and 402 ± 12 of O_2 (mg Chl)$^{-1}$ h^{-1}, for WT control, D1-D170E, D1-E189Q and D1-E189K respectively. Data were fit to Eq. 1 for parameter estimation. Error bars represent SD with n ≥ 3.

Table S1. Dark rearrangement, kA and decay of intermediates, kD, parametersof WT control, D1-D170E, D1-E189K, D1-E189R, and D1-E189Q mutant strains.

STRAIN	K_A (S^{-1}) ($T_{1/2}$)	K_D (S^{-1}) ($T_{1/2}$)	R
WT CONTROL	10.45 (66ms)	0.37 (1.8s)	0.97
D1-D170E	8.72 (79ms)	0.86 (0.8s)	0.99
D1-E189K	8.45 (82ms)	0.63 (1.1s)	0.95
D1-E189Q	8.86 (78ms)	0.55 (1.2s)	0.99

[a] Values of parameters were estimated from the fits of the flash interval data (Figure 3) using the into the equation (24,30) derived from the two-quantum model of photoactivation (Scheme 1) (33). Note that the number of photoactivation flashes were different among samples and were adjusted to produce 50% restoration of activity according to the fast phase of photoactivation (Figure 2). This corresponded to 150, 250, 350 and 500 for WT control, D1-E189Q, D1-E189K and D1-D170E respectively.

5.2. Fluorescence relaxation kinetics

The acceptor side forward electron flow from Q_A^- to Q_B site does not seem to be affected by Mn-depletion nor after photoactivation, even in the mutants (**Figs, S2A and S2E**) indicating an absence of acceptor side damage. However, the kinetics of charge recombination between the donor and acceptor side observed in the presence of DCMU in HA-treated cells indicate a significant alterations at the HAS in studied mutants. The D1-D170E and D1-E189K mutants displayed nearly complete decay of Q_A^- within 1s following HA-extraction of the Mn_4CaO_5 (**Fig. 2F, Table S2**). In contrast, the decay of fluorescence WT control was not complete even after over 100s. The longer lifetime of Q_A^- in the WT is due to the presence of Mn^{2+} at the HAS at the moment of the charge separation permitting efficient reduction of P_{680}^+ and thereby trapping the center in the high fluorescent $Y_ZP_{680}Q_A^-$ state (5, 19, 65). Although the Mn_4CaO_5 has been removed in the samples, there is a sufficient concentration of Mn^{2+} in the cells to allow full reassembly and therefore it is reasonable that Mn^{2+} can occupy the HAS in these samples.

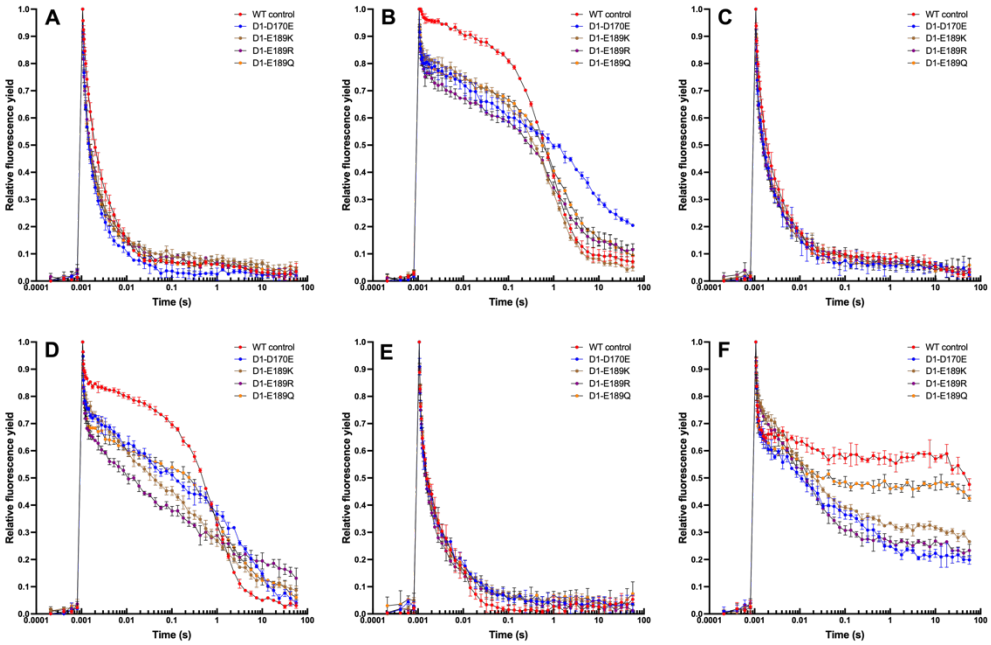

Figure S2. Q_A^- reoxidation kinetics in WT control, D1-D170E, D1-E189K, D1-E189R, and D1-E189Q strains in the (**A**) absence of DCMU, (**B**) presence of DCMU, (**C**) re-photoactivated cells in the absence of DCMU, (**D**) re-photoactivated cells in the presence of DCMU, **(E)** Mn-depleted cells in the absence of DCMU, **(F)** Mn-depleted cells in the absence of DCMU. For the purpose of the photoactivation (**C and D**) the sequence of 2000 single turnover flashes was given to the HA-extracted cyanobacterial cells at uniform interval at 2Hz (500ms flash interval). The measurements were performed after a single actinic flash of light. Samples were dark adapted for 5 minutes prior the measurements. Error bars represent SD with n ≥ 3.

Table S2. Characteristics of chlorophyll fluorescence relaxation kinetics in untreated and re-photoactivated WT control, D1-D170E, D1-E189K, D1-E189R and D1-E189Q cells.

Strain	Fast phase: τ/ms (amplitude (%))	Middle phase: τ/ms (amplitude (%))	Slow phase: τ/s (amplitude (%))	R
Intact Mn_4O_5Ca cluster in the absence of DCMU				
WT control	0.4 (86.9)	4.29 (11.1)	8.3 (1.9)	0.99
D1-D170E	0.3 (96)	7.4 (3.5)	86. 6 (0.5)	0.99
D1-E189K	0.2 (97.3)	5.2 (2)	34.8 (0.6)	0.99
D1-E189R	0.3 (95.8)	4.9 (3.3)	6.9 (0.9)	0.98
D1-E189Q	0.26 (96.8)	5.9 (2.6)	36.5 (0.7)	0.98
Intact Mn_4O_5Ca cluster in the presence of DCMU				
WT control	1.6 (11)	(0)-	0.75 (89)	0.99
D1-D170E	13.9 (24.8)	3008 (47.9)	>100 (27.2)	0.99
D1-E189K	3 (16)	(0)-	0.8 (75)	0.98
D1-E189R	3.9 (25.4)	(0)-	1.6 (74.5)	0.98
D1-E189Q	0.93 (28.9)	(0)-	1 (71)	0.99
Re-photoactivated cells in the presence of DCMU				
WT control	0.8 (21.8)	(0)-	0.7 (78.2)	0.99
D1-D170E	0.9 (23.5)	308 (26.9)	4.7 (49.6)	0.99
D1-E189K	5.6 (37.5)	627 (49.4)	>100 (13.1)	0.99
D1-E189R	3.7 (38.1)	269 (33.7)	96.9 (28.1)	0.99
D1-E189Q	2.36 (24)	1011 (63.3)	89.6 (12.6)	0.99
Mn-depleted cells in the presence of DCMU				

WT control	7.9 (14.5)	(0)-	> 100 (85.4)	0.99
D1-D170E	6.5 (39.5)	446 (27.9)	> 100 (32.5)	0.99
D1-E189K	5.9 (40.5)	144 (18.5)	> 100 (40.9)	0.99
D1-E189Q	0.27 (72.8)	15.8 (6.5)	> 100 (20.7)	0.98

For the purpose of photoactivation the sequence of 2000 single turnover flashes was given to the HA-extracted cyanobacterial cells at uniform interval at 2Hz (500ms flash interval). The decay curves in the absence of DCMU were fit assuming exponential decay for the fast and the middle phases and hyperbolic for the slow phase. The decay curves in the presence of DCMU were analyzed with exponential components for the fast decay and hyperbolic for the slow phase, except for D1-D170E where exponential fit was used for the fast phase and hyperbolic for both middle and slow phases. The data from re-photoactivated samples was analyzed with exponential fit for the fast phase and hyperbolic for both middle and slow phases except for WT control where an exponential component was used for the fast decay and hyperbolic for the slow phase (see Table 7). For Mn-depleted cells in the presence of DCMU the decay curves were analyzed by assuming exponential decay for the fast phase and hyperbolic for both middle and slow phases, except for WT control where exponential fit was used for the fast phase and hyperbolic for the slow phase (see Table 1).

Supplementary figures

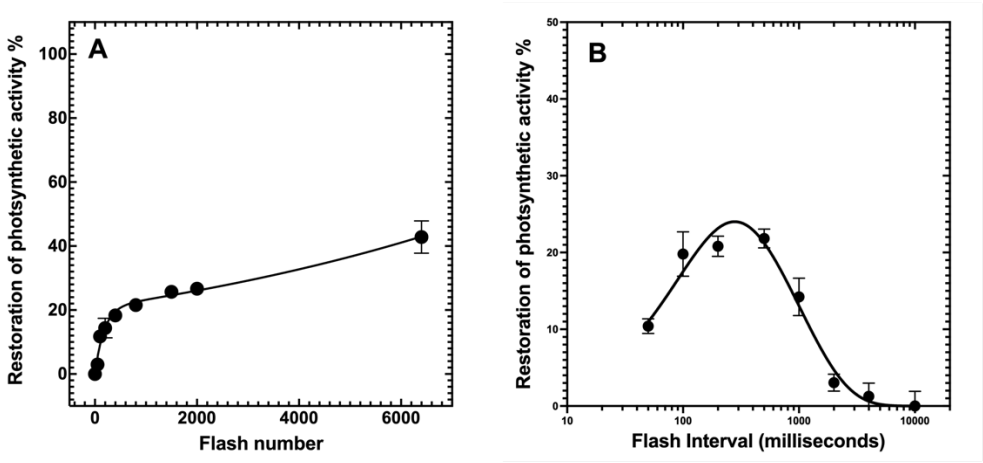

Figure S3. Photoactivation of HA-extracted cells as a function of (**A**) single-turnover flash number. Series of xenon lamp flashes were given at uniform frequency of 2 Hz (500ms flash interval) to hydroxylamine-treated D1-E189R cells. Kinetic fit parameters of $\boldsymbol{\Phi}_{PA1} = 5.7 \times 10^{-3}$ *and* $\boldsymbol{\Phi}_{PA2} = 1.1 \times 10^{-4}$ obtained from the data from the was fit into Equation 1. (**B)** Photoactivation of HA-extracted cells as a function of flash interval. Flashes were given at six different equal flash intervals to hydroxylamine-treated D1-E189R cells. The number of photoactivation flashes was determined based on the flash number experiment (**Fig. S1A**) to produce approximately 50% restoration of activity and corresponded to 350 flashes. Data were fit to Eq. 2 for parameter estimation. The percentage of O_2 evolution recovery was calculated as a fraction from the O_2 evolution rate prior HA extraction equals 262 ± 9 µmol of O_2 (mg Chl)$^{-1}$ h^{-1}. Error bars represent SD with n ≥ 3

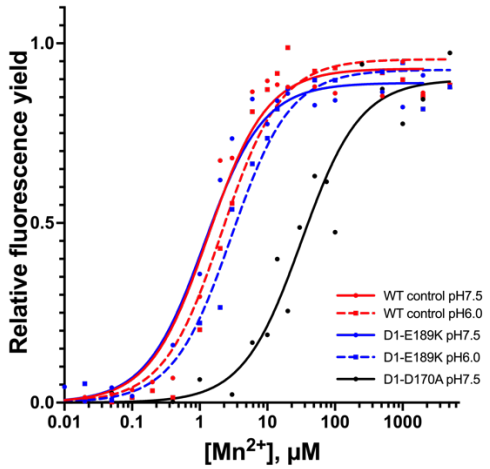

Figure S4. Electron donation in purified Mn-depleted PSII as a function of Mn^{2+} concentration. The variable fluorescence emitted by PSII from WT control, D1-E189K and D1-D170A strains at pH6.0 (dashed line) and pH7.5 (solid line) was measured after the excitation with saturating laser flashes (5ns, 300ms apart) (43). Sample contained 5µg of Chl\mL, 10µM 2,6- DCBQ as an external electron acceptor, pH 6.0). Fluorescence data was normalized to 1 and fit into Michaelis-Menten equation to derive K_m values. Every single data point represents an average of 3-5 technical repeats

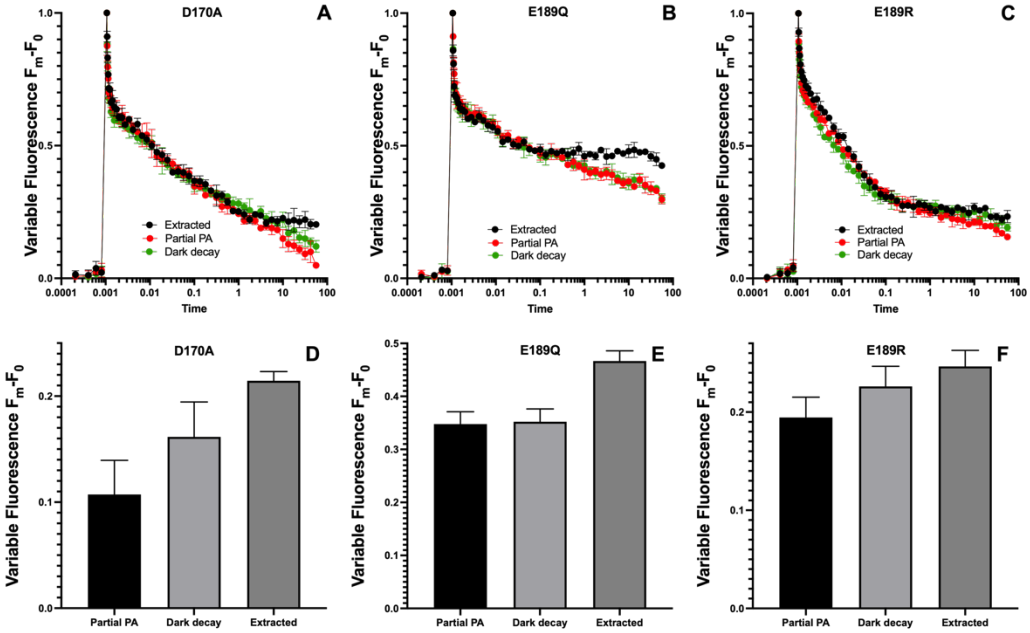

Figure S5. Q_A^- reoxidation kinetics in partially photoactivated **(A)** D1-D170E, **(B)** D1-E189Q, and **(C)** D1-E189R mutants in the presence of DCMU**.** For the purpose of the partial photoactivation the sequence of 300, 200 and 200 single turnover flashes was given to the HA-extracted cells at uniform interval at 2Hz (500ms flash interval), respectively. Dark incubated sample was stored in complete darkness on a rotary shaker for 40 minutes prior the measurements. Panels **(D)**, **(E)** and **(F)** show the relative difference in the fluorescence relaxation kinetics in WT control and D1-E189K prior photoactivation, after photoactivation and after the dark incubation, the average of the last 8 fluorescence datapoints from panels **(A), (B)** and **(C)** were taken to obtain the bar plots, higher level of fluorescence after the dark incubation indicates on a slower relaxation due to the absence of electron acceptor at the donor side of PSII. The measurements were performed after a single actinic flash of light. Samples were dark adapted for 5 minutes prior the measurements. Error bars represent SD with $n \geq 3$

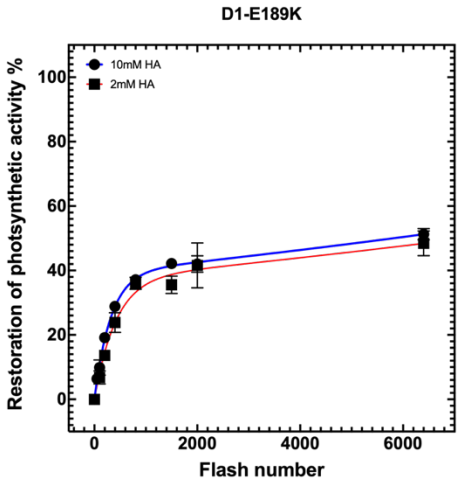

Figure S6. Photoactivation of HA-extracted cells as a function of the single-turnover flash number. Series of xenon lamp flashes were given at uniform frequency of 2 Hz (500ms flash interval) to D1-E189K treated with 2mM and 10mM hydroxylamine. The percentage of O_2 evolution recovery was calculated as a fraction from the O_2 evolution rate prior HA extraction 544 ± 16 µmol of O_2 (mg Chl)$^{-1}$ h^{-1}, Error bars represent SD with $n \geq 3$.

693 **Table S3.** Values of the variable fluorescence of the from WT control, D1-D170E, D1-E189K, D1-E189R and D1-
694 E189Q cells prior the HA extraction.

Strain	Fv (F_m-F_0/F_0)
WT control	0.78
D1-D170E	0.65
D1-E189K	0.65
D1-E189R	0.44
D1-E189Q	0.52

695 **Table S4.** Characteristics of chlorophyll fluorescence relaxation kinetics in partially photoactivated, D1-D170E, D1-
696 E189Q and D1-E189R cells.

Partially photoactivated cells in the presence of DCMU					
Strain/State		**Fast phase: τ/ms (amplitude (%))**	**Middle phase: τ/ms (amplitude (%))**	**Slow phase: τ/s (amplitude (%))**	**R**
D1-D170E	Extracted	6.5 (39.5)	446 (27.9)	> 100 (32.5)	0.99
	Partial Photoactivation	6 (36.9)	260 (27.9)	17.4 (35.3)	0.99
	Dark incubated	9.4 (40.7)	570 (18.7)	40.9 (38.9)	0.99
D1-E189R	Extracted	2.9 (33.7)	44 (35.1)	> 100 (32.6)	0.99
	Partial Photoactivation	4.9 (43.3)	144 (24.2)	91 (32.4)	0.99
	Dark incubated	1.76 (40.4)	36 (27.7)	> 100 (31.9)	0.99
D1-E189Q	Extracted	0.27 (72.8)	15.8 (6.5)	> 100 (20.7)	0.98
	Partial Photoactivation	6.2 (26.4)	551 (16.8)	> 100 (56.9)	0.99
	Dark incubated	7.4 (27.2)	760 (14.3)	> 100 (58.6)	0.99

697 For the purpose of the partial photoactivation the sequence of 300, 200 and 200 single turnover flashes was given to
698 the HA-extracted cells at uniform interval at 2Hz (500ms flash interval), respectively. The decay curves were analyzed
699 by assuming exponential decay for the fast phase and hyperbolic for both middle and slow phases, except for WT
700 control where exponential fit was used for the fast phase and hyperbolic for the slow phase (see Table 1).

701

1. G. T. Babcock *et al.*, Water oxidation in photosystem II: From radical chemistry to multielectron chemistry. *Biochemistry* **28**, 9557-9565 (1989).
2. T. Cardona, A. Sedoud, N. Cox, A. W. Rutherford, Charge separation in Photosystem II: A comparative and evolutionary overview. *Biochimica et Biophysica Acta (BBA) - Bioenergetics* **1817**, 26-43 (2012).
3. B. Kok, B. Forbush, M. McGloin, Cooperation of charges in photosynthetic O_2 evolution-I. A linear four step mechanism. *Photochem Photobiol* **11**, 457-475 (1970).
4. H. Bao, R. L. Burnap, Photoactivation: The light-driven assembly of the water oxidation complex of photosystem II. *Frontiers in Plant Science* **7**, 578 (2016).
5. T. A. Ono, H. Mino, Unique binding site for Mn^{2+} ion responsible for reducing an oxidized Y_Z tyrosine in manganese-depleted photosystem II membranes. *Biochemistry* **38**, 8778-8785 (1999).
6. G. M. Ananyev, A. Murphy, Y. Abe, G. C. Dismukes, Remarkable affinity and selectivity for Cs+ and uranyl (UO22+) binding to the manganese site of the apo-water oxidation complex of photosystem II. *Biochemistry* **38**, 7200-7209 (1999).
7. R. J. Boerner, A. P. Nguyen, B. A. Barry, R. J. Debus, Evidence from directed mutagenesis that aspartate 170 of the D1 polypeptide influences the assembly and-or stability of the manganese cluster in the photosynthetic water-splitting complex. *Biochemistry* **31**, 6660-6672 (1992).
8. P. J. Nixon, B. A. Diner, Aspartate 170 of the photosystem II reaction center polypeptide D1 is involved in the assembly of the oxygen evolving manganese cluster. *Biochemistry* **31**, 942-948 (1992).
9. P. J. Nixon, J. T. Trost, B. A. Diner, Role of the carboxy terminus of polypeptide-D1 in the assembly of a functional water-oxidizing manganese cluster in photosystem-II of the cyanobacterium *Synechocystis sp* PCC6803 - assembly requires a free carboxyl group at C-terminal position 344. *Biochemistry* **31**, 10859-10871 (1992).
10. H. A. Chu, A. P. Nguyen, R. J. Debus, Site-directed Photosystem-II mutants with perturbed oxygen-evolving properties .2. Increased binding or photooxidation of manganese in the absence of the extrinsic 33-kda polypeptide in-vivo. *Biochemistry* **33**, 6150-6157 (1994).
11. R. O. Cohen, P. J. Nixon, B. A. Diner, Participation of the C-terminal region of the D1-polypeptide in the first steps in the assembly of the Mn4Ca cluster of photosystem II. *Journal of Biological Chemistry* **282**, 7209-7218 (2007).
12. G. M. Ananyev, G. C. Dismukes, High-resolution kinetic studies of the reassembly of the tetra-manganese cluster of photosynthetic water oxidation: proton equilibrium, cations, and electrostatics. *Biochemistry* **35**, 14608-14617 (1996).
13. P. J. Nixon, B. A. Diner, Analysis of water-oxidation mutants constructed in the cyanobacterium *Synechocystis sp.* PCC6803. *Biochem Soc Trans* **22**, 338-343 (1994).
14. Y. Umena, K. Kawakami, J. R. Shen, N. Kamiya, Crystal structure of oxygen-evolving photosystem II at a resolution of 1.9 Ångstrom. *Nature* **473**, 55-U65 (2011).
15. C. J. Gisriel *et al.*, Cryo-EM structure of monomeric photosystem II from *Synechocystis sp* PCC 6803 lacking the water-oxidation complex. *Joule* **4**, 2131-2148 (2020).
16. J. Zabret *et al.*, Structural insights into photosystem II assembly. *Nat Plants* **7**, 524-538 (2021).
17. S. Nakamura, T. Noguchi, Initial Mn2+ binding site in photoassembly of the water-oxidizing Mn4CaO5 cluster in photosystem II as studied by quantum mechanics/molecular mechanics calculations. *Chemical Physics Letters* **721**, 62-67 (2019).
18. C. G. Chen, J. Kazimir, G. M. Cheniae, Calcium modulates the photoassembly of photosystem-II (MN)(4)-cluster by preventing ligation of nonfunctional high-valency states of manganese. *Biochemistry* **34**, 13511-13526 (1995).
19. R. J. Debus, K. A. Campbell, D. P. Pham, A.-M. A. Hays, R. D. Britt, Glutamate 189 of the D1 polypeptide modulates the magnetic and redox properties of the manganese cluster and tyrosine Y_Z in photosystem II. *Biochemistry* **39**, 6275-6287 (2000).
20. H. A. Chu, A. P. Nguyen, R. J. Debus, Amino-acid-residues that influence the binding of manganese or calcium to photosystem-II.1. The lumenal intehelical domains of the D1 polypepride. *Biochemistry* **34**, 5839-5858 (1995).
21. C. Tommos, G. T. Babcock, Proton and hydrogen currents in photosynthetic water oxidation. *Biochimica et Biophysica Acta (BBA) - Bioenergetics* **1458**, 199-219 (2000).
22. C. Tommos, G. T. Babcock, Oxygen production in nature: A light-driven metalloradical enzyme process. *Accounts of Chemical Research* **31**, 18-25 (1998).

23. H. A. Chu, A. P. Nguyen, R. J. Debus, Amino-acid-residues that influence the binding of manganese or calcium to photosystem-II.2. The carboxy-terminal domain of the D1 polypeptide. *Biochemistry* **34**, 5859-5882 (1995).
24. M. Ibrahim *et al.*, Untangling the sequence of events during the S2 --> S3 transition in photosystem II and implications for the water oxidation mechanism. *Proc Natl Acad Sci USA* **117**, 12624-12635 (2020).
25. M. Suga *et al.*, Light-induced structural changes and the site of O=O bond formation in PSII caught by XFEL. *Nature* 10.1038/nature21400 (2017).
26. P. E. Siegbahn, Water oxidation mechanism in photosystem II, including oxidations, proton release pathways, O-O bond formation and O_2 release. *Biochimica et biophysica acta* **1827**, 1003-1019 (2013).
27. N. Cox *et al.*, Electronic structure of the oxygen-evolving complex in photosystem II prior to O-O bond formation. *Science* **345**, 804-808 (2014).
28. M. Ibrahim *et al.*, Untangling the sequence of events during the S2 --> S3 transition in photosystem II and implications for the water oxidation mechanism. *Proceedings of the National Academy of Sciences of the United States of America* **117**, 12624-12635 (2020).
29. Y. Kanesaki *et al.*, Identification of substrain-specific mutations by massively parallel whole-genome resequencing of *Synechocystis sp* PCC 6803. *DNA research : an international journal for rapid publication of reports on genes and genomes* **19**, 67-79 (2012).
30. R. J. Debus *et al.*, Does histidine 332 of the D1 polypeptide ligate the manganese cluster in photosystem II? An electron spin echo envelope modulation study. *Biochemistry* **40**, 3690-3699 (2001).
31. H. A. Chu, A. P. Nguyen, R. J. Debus, Site-directed Photosystem-ii mutants with perturbed oxygen-evolving properties .1. Instability or inefficient assembly of the manganese cluster in-vivo. *Biochemistry* **33**, 6137-6149 (1994).
32. J. G. K. Williams, "Construction of specific mutations in photosystem II photosynthetic reaction center by genetic engineering methods in *Synechocystis 6803*" in Methods in Enzymology. (Academic Press, 1988), vol. 167, pp. 766-778.
33. G. M. Cheniae, I. F. Martin, Effect of hydroxylamine on Photosystem-II .1. Factors affecting decay of O2 evolution. *Plant Physiology* **47**, 568-& (1971).
34. H. J. Hwang, R. L. Burnap, Multiflash experiments reveal a new kinetic phase of photosystem II manganese cluster assembly in *Synechocystis sp.* PCC6803 *in vivo*. *Biochemistry* **44**, 9766-9774 (2005).
35. H. J. Hwang, A. McLain, R. J. Debus, R. L. Bumap, Photoassembly of the manganese cluster in mutants perturbed in the high affinity Mn-binding site of the H_2O-oxidation complex of photosystem II. *Biochemistry* **46**, 13648-13657 (2007).
36. R. Radmer, G. M. Cheniae, Photoactivation of manganese catalyst of O_2 evolution .2. 2-Quantum mechanism. *Biochimica et biophysica acta* **253**, 182-& (1971).
37. A. P. Avramov, H. J. Hwang, R. L. Burnap, The role of Ca^{2+} and protein scaffolding in the formation of nature's water oxidizing complex. *Proceedings of the National Academy of Sciences* **117**, 28036 (2020).
38. A. F. Miller, G. W. Brudvig, Manganese and calcium requirements for reconstitution of oxygen evolution activity in manganese-depleted photosystem II membranes. *Biochemistry* **28**, 8181-8190 (1989).
39. N. Tamura, G. Cheniae, Photoactivation of the water-oxidizing complex in photosystem II membranes depleted of Mn and extrinsic proteins. I. Biochemical and kinetic characterization. *Biochimica et biophysica acta* **890**, 179-194 (1987).
40. I. Vass, D. Kirilovsky, A.-L. Etienne, UV-B radiation-induced donor- and acceptor-side modifications of photosystem II in the cyanobacterium *Synechocystis sp.* PCC 6803. *Biochemistry* **38**, 12786-12794 (1999).
41. K. Cser, B. A. Diner, P. J. Nixon, I. Vass, The role of D1-Ala344 in charge stabilization and recombination in photosystem II. *Photochemical & photobiological sciences : Official journal of the European Photochemistry Association and the European Society for Photobiology* **4**, 1049-1054 (2005).
42. R. L. Burnap, M. Qian, C. Pierce, The manganese-stabilizing protein of photosystem II modifies the in vivo deactivation and photoactivation kinetics of the H_2O oxidation complex in *Synechocystis sp* PCC6803. *Biochemistry* **35**, 874-882 (1996).
43. P. Chernev *et al.*, Light-driven formation of manganese oxide by today's photosystem II supports evolutionarily ancient manganese-oxidizing photosynthesis. *Nature Communications* **11**, 6110 (2020).
44. B.-D. Hsu, J.-Y. Lee, R.-L. Pan, The high-affinity binding site for manganese on the oxidizing side of Photosystem II. *Biochimica et Biophysica Acta (BBA) - Bioenergetics* **890**, 89-96 (1987).
45. C. W. Hoganson, D. F. Ghanotakis, G. T. Babcock, C. F. Yocum, Manganese ion reduces redox activated tyrosine in manganese-depleted photosystem II preparations. *Photosynth Res* **22**, 285-294 (1989).

46. B. K. Semin, M. Seibert, A carboxylic residue at the high-affinity, Mn-binding site participates in the binding of iron cations that block the site. *Biochim Biophys Acta* **1757**, 189-197 (2006).
47. B. K. Semin, M. Seibert, Flash-induced blocking of the high-affinity manganese-binding site in photosystem II by iron cations: dependence on the dark interval between flashes and binary oscillations of fluorescence yield. *J Phys Chem B* **110**, 25532-25542 (2006).
48. D. J. Vinyard *et al.*, Photosystem II oxygen-evolving complex photoassembly displays an inverse H/D solvent isotope effect under chloride-limiting conditions. *Proceedings of the National Academy of Sciences* **116**, 18917 (2019).
49. C. A. Tracewell, A. Cua, D. H. Stewart, D. F. Bocian, G. W. Brudvig, Characterization of Carotenoid and Chlorophyll Photooxidation in Photosystem II. *Biochemistry* **40**, 193-203 (2001).
50. T. A. Ono, Y. Inoue, Requirement of divalent cations for photoactivation of the latent water oxidation system in intact chloroplasts from flashed leaves. *Biochimica et biophysica acta* **723**, 191-201 (1983).
51. A. M. Tyryshkin *et al.*, Spectroscopic Evidence for Ca2+ Involvement in the Assembly of the Mn4Ca Cluster in the Photosynthetic Water-Oxidizing Complex. *Biochemistry* **45**, 12876-12889 (2006).
52. D. A. Weisz *et al.*, A novel chlorophyll protein complex in the repair cycle of photosystem II. *Proceedings of the National Academy of Sciences* **116**, 21907 (2019).
53. K. Becker, K. U. Cormann, M. M. Nowaczyk, Assembly of the water-oxidizing complex in photosystem II. *J Photochem Photobiol B* **104**, 204-211 (2011).
54. P. J. Nixon, M. Barker, M. Boehm, R. de Vries, J. Komenda, FtsH-mediated repair of the photosystem II complex in response to light stress. *Journal of Experimental Botany* **56**, 357-363 (2005).
55. R. Burnap, L. A. Sherman, Deletion mutagenesis in Synechocystis sp. PCC6803 indicates the the Mn-stabilizing protein of photosystem II is not essential for O2 evolution. *Biochemistry* **30**, 440-446 (1991).
56. H. Bao, R. L. Burnap, Photoactivation: The light-driven assembly of the water oxidation complex of photosystem II. *Front Plant Sci* **7**, 578 (2016).
57. E. Busch, E. Hohenester, R. Timpl, M. Paulsson, P. Maurer, Calcium Affinity, Cooperativity, and Domain Interactions of Extracellular EF-hands Present in BM-40*. *Journal of Biological Chemistry* **275**, 25508-25515 (2000).
58. M. Zhang *et al.*, Structural insights into the light-driven auto-assembly process of the water-oxidizing Mn4CaO5-cluster in photosystem II. *Elife* **6** (2017).
59. C. Chen, J. Kazimir, G. M. Cheniae, Calcium modulates the photoassembly of photosystem II (Mn)4 clusters by preventing ligation of nonfunctional high valency states of manganese. *Biochemistry* **34**, 13511 13526 (1995).
60. P. Chernev *et al.*, Light-driven formation of manganese oxide by today's photosystem II supports evolutionarily ancient manganese-oxidizing photosynthesis. *Nat Commun* **11**, 6110 (2020).
61. G. M. Cheniae, I. F. Martin, Photoactivation of the manganese catalyst of O_2 evolution. I. Biochemical and kinetic aspects. *Biochimica et biophysica acta* **253**, 167-181 (1971).
62. T. Tokano, Y. Kato, S. Sugiyama, T. Uchihashi, T. Noguchi, Structural Dynamics of a Protein Domain Relevant to the Water-Oxidizing Complex in Photosystem II as Visualized by High-Speed Atomic Force Microscopy. *The Journal of Physical Chemistry B* 10.1021/acs.jpcb.0c03892 (2020).
63. G. M. Ananyev, G. C. Dismukes, Assembly of the tetra-Mn site of photosynthetic water oxidation by photoactivation: Mn stoichiometry and detection of a new intermediate. *Biochemistry* **35**, 4102-4109 (1996).
64. T.-A. Ono, Y. Inoue, Reductant-sensitive intermediates involved in multi-quantum process of photoactivation of latent O_2-evolving system. *Plant and Cell Physiology* **28**, 1293-1299 (1987).
65. B. A. Diner, P. J. Nixon, The rate of reduction of oxidized redox-active tyrosine, Z+, by exogenous Mn2+ is slowed in a site-directed mutant, at aspartate 170 of polypeptide D1 of photosystem II, inactive for photosynthetic oxygen evolution. *Biochimica et Biophysica Acta (BBA) - Bioenergetics* **1101**, 134-138 (1992).